Structural, Optical and Magnetic Properties of Nickel-Copper Ferrite $Ni_xCu_{1-x}Fe_2O_4$

Ferydon Babaei (fbabaei@qom.ac.ir)
University of Qom https://orcid.org/0000-0003-1704-0474
Afroz Ghasemi
University of Qom

Research Article

Keywords: nanoparticles, ferrite, combustion

Posted Date: September 28th, 2021

DOI: https://doi.org/10.21203/rs.3.rs-895859/v1

Abstract

Nickel-copper ferrite nanoparticles $Ni_xCu_{1-x}Fe_2O_4$ with values x = 0.3, 0.5,0.7 fabricated by combustion method . X-ray diffraction (XRD) analyzes confirmed the formation of the ferrite structure. The average size of crystals was estimated to range from 39 to 44 nm. The particle morphology was detected and interpreted by the FSEM scanning microscope and the porosity characteristic of the ferrite structure based on the combustion method was observed. The FTIR analysis was performed to investigate the bonds in which the tensile vibrational mode of the tetrahedral site in the range of the wavelength of 500-600 cm^{-1} .The magnetic properties of nanoparticles were investigated using VSM analysis and the effect of increasing of copper ion on M_S saturation magnetization and H_C coercivity force was investigated. With respect to the saturation magnetization values for the synthesized samples, it was observed that by increasing the Cu content from x = .3 to x = .5 the saturation magnetization decreased and then increasing with increasing Cu content such that at x = .5, we had the lowest saturation magnetism. Reduction of saturation magnetization Copper ions occupy ferric ions in tetrahedral sites and iron ions are transferred to octahedral sites. The results of UV-Vis indicate to complete absorption in the samples. The linearity of the edge of the absorption spectrum relates to a direct energy band gap and the effect of increasing copper ions on ferrite conductivity was investigated.

1. Introduction

Soft ferrite is widely used for many types of magnetic devices such as high frequency transformers, inductors and magnetic heads; because, they have higher electrical resistance compared to soft magnetic alloys. Various replacements have been taken into consideration in order to achieve the desirable electrical and magnetic properties. Useful range of ferrite frequency is limited to the beginning of resonance phenomenon within which permeability in critical frequency would be reduced. Therefore, information related to dependency of frequency to initial permeability is required. Many cases of research have been performed on magnetic spectrum of different types of ferrites within wide range of frequency [1–8]. Those groups of magnetic materials main component of which being ferric oxide and having ferrimagnetic properties are called ferrite; also, from among main characteristics of them can be made to desirable magnetic parameters such as magnetic permeability coefficient, saturated induction and high specific electrical resistance (about 1012 Ω). Ferrite nanocrystals doped with different divalent metals like chrome, copper, manganese, and zinc are highly used due to improvement made in some of their electrical properties [9–11]; and, copper or zinc-substituted nickel ferrite shows more improvement as a soft magnetic material [12].

Soft magnetic ferrites are usually produced through solid-state method due to simplicity of process [13]; however, these methods are seriously limited in producing fine-grained powders in nano size [14]. New methods like combustion synthesis have been developed to overcome above limitations. Glycine-nitrate process in which glycine is used as fuel and nitrate as an oxidant is a quick and low cost method done with few numbers of equipment so that homogeneous nanoparticles with high crystallinity percentage would be produced [15]. Combustion method is based on combustion of an aqueous solution including

desirable metallic salts (usually nitrates) and some amounts of organic fuels. Considerable aspect of combustion method concerns very good and homogeneous mixture of reaction components through usage made of one fuel and proper complexing agent (citric acid, urea, glycine, and etc.); and, using an aqueous solvent as a reaction intermediate, exothermic reaction between fuel and oxidant material will take place. In general, a good fuel has to react without being volatile; and, it has to produce non-toxic gases and be able to act as a complexing agent for metal cations [16].

Instability factors of Nano-ferrites are affected by interplay of their crystal and magnetic structures. Studying the behavior and above inter-mutual properties shows high sensitivity to fabrication method of magnetic nanoparticles and their size in nano-scale magnetic fields. In the research and after making nickel-copper ferrites ($Ni_xCu_{1-x}Fe_2O_4$) through combustion method with different weight percentages; their structural, optical and magnetic properties have been studied. In Sect. 2, the experiment method is presented, followed by the results and analyses in Sect. 3.

2. Experiment Method

To fabricate $Ni_xCu_{1-x}Fe_2O_4$ nanoparticles with various values of x = 0.3, 0.5, and 0.7, raw materials including Nickel(II) nitrate hexahydrate ($Ni(NO_3)_2.6H_2O$), copper (II) nitrate hexahydrate ($Cu(NO_3)_2.\ 6H_2O$), Iron(III) nitrate nonahydrate ($Fe(NO_3)_3.9H_2O$) and glycine ($C_2H_5NO_2$), all of which purchased from Merck Co. have been used. Required amounts of zinc, copper, and iron nitrates have been weighted by gravimetric calculations, using digital scale; then, they have been poured in the beaker. Considering selection of fuel ratio to nitrate being equal to 0.5, glycine amount has been calculated and weighted; then, it has been poured in the beaker. Proper amount of water (40 cc) has been poured in the beaker; then, the beaker containing these materials has been put on heater. Primarily water inside the beaker has been vaporized and after almost 25 minutes averagely calculated for three samples, spontaneous combustion has been occurred. Within a few seconds, a dark brown porous fragile material would be produced which is the same ferrite concerned. Images related to the aforementioned spontaneous combustion and fabricated ferrite is presented in Fig. 1.High gas pressure at time of exit causes porosity to be created; so, final product includes micro particles with very low particle accumulation. This lack of accumulation will lead to large site occupied by particles. Therefore, using mortar we make particles to occupy less space.

In gravimetric calculations, molar mass of each of these chemical compounds has been used. To fabricate nickel-copper ferrite, 2 to 1 relationship of iron nitrate and total amounts of nickel and copper nitrates have been dissolved in distilled water with consideration of molar mass of each as well as x value. In order for prepared material to be enough for various tests, 0.2 mole of Iron nitrate (4.04gr) and 0.01 mole nickel and copper nitrate (0.532gr) have been considered; while, nickel and copper amounts have been weighted with consideration of x value. That is 0.023 + 0.012 = 0.08 mole nitrate. Considering glycine-nitrate ratio (G/N = 0.5), glycine weight has been calculated; and, 0.04 mole glycine would be equal to 3.0028gr. For example, in preparing $Ni._7Cu._3\ Fe_2O_4$ and with consideration of the method

explained, 0.007 mole nickel nitrate, 0.003 mole copper nitrate and 0.02 mole iron nitrate have been weighted and poured into the beaker.

X-ray diffraction pattern of samples has been analyzed by Philips X-ray diffractometer under radiation of CuKα on 1.54 A° wavelength. Morphological study of powders has been performed through FESEM images (Hitachi S4160). Magnetic properties have been studied by VSM device under 25 Hz frequency. FTIR analysis has been performed by infrared spectroscopy (VERTEX 70) and UV-Vis spectroscopy has been done by double beam spectrophotometry (Hitachi U-3501).

3. Results And Analyses

To study phases available in nanopowder fabricated from samples, XRD analysis within the range of 10–120 has been used. Figure 2 shows that clear peaks of X-ray diffraction corresponding to main reflection planes (220), (311), (400), (422), (511), and (440) are indicative of cubic spinel structure with Fd3m site group; and, availability of lattice sub planes (331), (222), and (111) is well matched with cubic spinel JCPDS diffraction file. Also, XRD analysis shows that main phase formed in the samples is Ferrite phase and line broadening shows nanometric structure of samples. Using Scherrer equation:

$$P_{hkl} = \frac{0.9\lambda}{\beta_{1/2}\cos\theta_{hkl}} \quad (1)$$

and peak (311), average size of crystallites can be estimated, where, radiated wavelength is 1.54 Å (Cu-Kα radiation), β1/2 is half of the peak width (rad) and θ_{ijk} is diffraction angel. With consideration of peaks (511) and (440) and using distance of planes as well as corresponding (hkl) Miller indices, lattice constant will be obtained from following equation:

$$\frac{\sin^2\theta}{h^2+k^2+l^2} = \frac{\lambda^2}{4a^2} \quad (2)$$

Considering the point that upon θ increase, error in the lattice constant would be reduced, mean of the two lattice constants related to bigger angels has been obtained; and, the related results are provided in Table.1. According to the values provided in the table, it is observed that lattice constants related to three samples of synthesized nickel-copper ferrites which can be considered as copper doped nickel ferrite are compatible with values of nickel and copper ferrites lattice constants provided in the reference [17]. In the table, crystallite size, lattice constant, lattice strain, and percentage of crystallization are reported as well.

Size of obtained particles with consideration of XRD results are from 39 to 44 nm. So, formation of nanoparticles with size of particles or crystallites is confirmed. It is also shown in Table.1 that increase of copper ion and decrease of nickel ion would be resulted in changes and contrast between particle size and magnetic energy. In second sample, balance would be made between the above changes so that order and stability of structure would be resulted in it. In second sample, maximum crystallite size is

observed; and, observing the column strain values cited in it, lowest lattice strain value is also related to the second sample. This is correct and confirmed with consideration of inverse dependence between strain and crystallite size. Considering $V = a^3$ (V is volume and a is lattice constant) the sample with lower volume is more stable; and, this is consistent with previous analyses performed in relation to the second sample. In general, it can be suggested that higher order in the lattice is related to higher crystallite size and lower lattice constant observed in the second sample. Upon increase of copper, lattice constant would be increased which can be related to Ni^{2+}(0.69Å) having smaller radius being replaced with Cu^{2+} (0.72Å) ions with bigger radius. This is consistent with references [18–21]. Also upon increase of Cu in the samples, it is observed that XRD angles of diffraction peak (311) will show tendency towards lower values which can be due to the point that in increasing trend, Cu value in lattice constant would be also increased. The reason is that, changes in particle size and magnetic energy which is observed upon Cu increase here will lead to replacement of particles and changes of angles. High crystallinity of samples is indicative of structural durability and stability of samples.

To study size, shape of particles and distribution of synthesized particles, FESEM (field emission scanning electron microscope) has been applied. The images in Fig. 3 show that the clusters are composed of fine particles. As far as no distributor has been used; formation of agglomeration is due to magnetic interaction and high reactivity expected in nanoparticles. This characteristic has been observed in all of the nanoparticles [22]. Samples on the surface are highly porous which can be attributed to quick exit of high volume of gases produced during combustion. Availability of porous lattice is one of characteristics of producing nanoparticles by combustion method. This porosity can be observed in nano and also bulk scales respectively with consideration of left and right images in Fig. 3. Particle size with consideration of images is within 30–60 nanometer range which is consistent with the results from crystallites in XRD analysis (Table.1).

FTIR transmission spectra are shown in Fig. 4 to study chemical bonds and to specify type of functional groups available in the compound. The bands in wavenumber about 548–560 cm^{-1} are related to vibrating-stretching mode of Fe ions located in tetrahedral site of the lattice with oxygen. Absorption band about 400–500 cm^{-1} is related to stretching fluctuation of Fe in octahedral site which cannot be observed due to device limitations; and, this is indicative of spinel phase formed in nickel-copper ferrite. Stretching/bending fluctuation mode of nitrate group NO_3^- within the wavenumber range of 1380 cm^{-1} and also within the wavenumber range of 1569–1653 cm^{-1} is related to carboxyl group COO^-; and, within the wavenumber range of 2331–2348 cm^{-1} and 3410–3446 cm^{-1}, it is related to bond stretching of water molecule as well as fluctuations of hydroxyl functional group (O-H) [23–25]. Changes of wavenumber of sites are dependent on cationic mass related to oxygen-cation distance and bonding force between magnetic ions located in sub lattices. Considering changes of wavenumber of tetrahedral site in Table.1, increase of copper ion in compound will lead to wavenumber displacement towards lower frequencies. Since changes of wavenumber has inverse relation with bond length; through increase of unit cell and bond length of Fe^{3+}- O^{2-} in tetrahedral sites, displacement towards less wavenumbers can be justified [26].

For magnetization measurement of samples at room temperature, an AGFM device (maximum 10kOe) has been used. The hysteresis loop of samples at room temperature have been shown in Fig. 5. Also, changes of coercivity(H_c), retentivity(M_r) and saturation magnetization(M_s) with changes in copper substitution amount in ferrite nanoparticles are provided in Table.2. Based on theory of Neel ferrimagnetism in spinel structure, cations are located in two different tetrahedral (A) and octahedral (B) sub lattices; and, magnetic moments of ions in each sub lattice are in parallel orientation; while, they are antiparallel in relation to each other. Considering the theory and knowing that magnetic moments of Fe^{+3}, Ni^{+2}, and $Cu^{+2}$are respectively equal to 7.1, 5, and 3.2μ_s [25], magnetic behavior of samples can be justified. One the hand, Ni^{+2} has strong dependence on octahedral site B and usually occupies the site. Cu^{+2} also prefers octahedral site; however, tetrahedral site A is shown to be occupied by it. Fe^{+3} also exists in both sites [27]. Considering values cited in saturated magnetization column in Table.2 for synthesized samples it is seen that when Cu increase from x = .3 to x = .5, saturated magnetization would be reduced. In continuation, through increase of Cu, the value would be increased i.e. in x = .5 minimum the saturated magnetization will be observed. In relation to reduction of saturated magnetization from x = .3 to .5 it can be suggested that upon increase of Cu, Cu^{+2} ions in tetrahedral sites A will be substituted Fe^{+3} ions. This way, Fe^{+3} ions will go from tetrahedral site A to octahedral site. Therefore, magnetic moment in site A as well as superexchange interaction between two sub lattices A and B would be reduced, reaching its minimum value in x = .5. Also, due to concentration increase in Fe^{+3} in octahedral sites B, number of Fe^{+3} and Fe^{+2} pairs will be increased which by itself will lead to anion vacancies in the lattice. These vacancies will lead to reduction of superexchange interaction and reduction of saturated magnetization, as a result. As for the samples, saturated magnetization will be increased from x = .5 to .7. This way, it can be suggested that in ferrites and through increase of one ion with lower magnet in one position, spin canting in opposite position will be created [19]. Considering reduction of magnetic moment of tetrahedral site A, due to increase of copper ion in this position and transfer of Fe^{+3} to octahedral site B, spin canting will happen. That is, spins in position A can no longer keep spins in position B powerfully in antiparallel form. As a result, moments in both sites will be no more parallel and spin canting will be observed in site B. Therefore, magnetization B will be reduced and considering the point that total saturated magnetization will be resulted from difference of saturated magnetization of octahedral site B and tetrahedral site A [20], total saturated magnetization will be increased upon reduction of saturated magnetization. When particle size changes to nanoscale, cation distribution in both A and B positions would be changed as well. There are various of superexchange interactions among positions A and B including J_{AA}, J_{BB}, and J_{AB}. Competition between these interactions is determinant of magnetization level of material. When particle size becomes close to nanoscale, quantum tunneling, cation redistribution and surface spin canting will be effective on physical characteristics of ferrite more than ever.

Comparing bulk and nano scales, when particle size becomes close to nanoscale, surface spin canting will lead to reduction of saturated magnetization in the samples. Also, disordered nanoparticle spins on surface prevent more internal spins to be oriented completely; and, they will lead to reduction of saturated

magnetization in nanoparticles. On the other hand, when particle size is reduced, number of domains will be reduced to a certain size in which the particle has been created only from one domain. Upon reduction particle size, coercive force in material will be increased to its maximum value; because, force required for change of spin orientation in single domain is much bigger than that required for movement of walls. Coercive force is affected by different factors such as defects, surface effects, pressures, non-magnetic atoms, and etc. On the other hand, growth of particles and substitution of less magnetic copper ion with iron in the compound will lead to reduction of interaction between magnetic particles as well as reduction of resistance in domains walls. Therefore, coercive force will be reduced [21, 22].

UV-Vis absorbance spectra and absorbance coefficient of ferrite nanoparticles with three different weight percentages are shown in Fig. 6. As observed, the optical absorbance which shows complete absorption at low wavelengths in samples. Sudden change in one certain wavelength confirms presence of energy band; and, as far as the graph is linear at absorption limit, energy gap is direct [28].

Direct and indirect optical gap can be calculated through equation.3, where, hv is photon energy, E_g is gap energy, n depends on nature of transfer and theoretically is equal to 1 and 1/2. α_0 is a fixed absorbance coefficient resulted from analysis of UV-Vis absorbance spectra. It has to be noted that absorbance coefficient and absorbance are linear proportionate and different in one constant value.

$$a(v) = \alpha_0(hv - E_g)^n / hv \quad (3)$$

Considering equation.4, $(\alpha(v)hv)^{1/n} / hv$ will be drawn based on hv and in accordance with the results from UV-Vis spectra, graph of which is provided in Fig. 6b.

$$(a(v)hv)^{1/n} = \alpha_0(hv - E_g) \quad (4)$$

Then equation.4 will be equalized to zero and/or the intercept to the tangent line of linear part of graph with horizontal axis will be obtained as values of gap energy. Values of direct gap energy n = 1/2 for nickel-copper ferrite particles with 0.7, 0.5, and 0.3 Percentages are respectively equal to 4.12, 3.91, and 3.60 eV. Values of gap energy are affected by different factors such as crystallite size, structural parameters, and presence of impurity. It is observed that upon increase of Cu, gap energy would be reduced. As referred to before, Ni^{+2} is highly dependent on site of octahedral B and usually occupies the position. Upon increase of Cu, Cu^{+2} ions will substitute Fe^{+3} ions in tetrahedral A site. Fe^{+3} ions will go from site of tetrahedral A to site of octahedral B. This will lead to increase of Fe^{+3} concentration in site B. As a result; while, numbers of Fe^{+3} and Fe^{+2} pairs will be increased which by itself causes creation of anion vacancies in the lattice. Conduction mechanism in ferrite is considerably affected by transfer of electron holes between Fe^{+3} and Fe^{+2} at octahedral B site. Here, it is observed that upon increase of Cu, gap energy would be reduced i.e. conduction will be increased.

4. Conclusions

Ferrite nanoparticles $Ni_x Cu_{1-x}Fe_2O_4$ (x = 0.3,0.5, 0.7) were fabricated by combustion method with glycine fuel. Presence of clear X-ray diffraction peaks corresponding to the main reflection planes in XRD patterns of samples confirmed the formation of nanoparticle with cubic spinel structure. The formation of ferrite phase based on FTIR results related to presence vibration mode Fe ions located at lattice tetrahedral site with Oxygen is also verifiable. Combustion materials are very porous and therefore have a large surface area, which can be clearly seen in FESEM images, which is due to the release of large volumes of gases during the process. The results of calculating the particle size synthesized using both SEM and XRD analysis are in agreement with each other. The results of VSM show that the magnetic behavior of nanoparticles depends on the effect of increasing copper ions and decreasing the amount of nickel. By increasing the value of Cu from x = 0.3 to x = 0.5, the amount of saturation magnetization decreases and then with increasing the amount of Cu, this value increases so that at x = 0 .5 we see the lowest saturation magnetization. These changes were explained by the placement of copper and nickel ions in the tetrahedral and octahedral sites and in terms of the exchange interactions between the sites and also the spin canting. The direct gap energy was calculated using the UV result. The rate of copper dopant on conduction was studied so that the energy gap increases, the conduction decreases by increasing the amount of copper which is well compatible with the conduction mechanism.

Declarations

Acknowledgement

This work was carried out with the support of the University of Qom.

-Funding

Not applicable.

-Competing interests

The authors declare no competing interests. The authors alone are responsible for the

content and writing of this article.

-Code availability

Not applicable.

-Authors' contributions

Ferydon Babaei: Investigation, Writing original draft, Formal analysis, Experiment

Afroz Ghasemi: Experiment, Writing.

- Ethics approval

All analyses were based on previous published studies, experimental and theoretical simulation, thus no ethical approval and patient consent are required.

-Consent to participate

Written informed consent for publication was obtained from all participants. The authors consented to participate.

-Consent for publication

Written informed consent for publication was obtained from all participants. The authors consented to publish.

References

1. G.T., Rado, R.W., Wright, and Emerson, W.H., Ferromagnetism at very high frequencies. III. Two mechanisms of dispersion in a ferrite, Phys. Rev. 80(1950) 273
2. G.T., Rado, Magnetic spectra of ferrites, Rev. Mod. Phys. 25 (1953) 81
3. Smit, J., Wijn, H.P.J., Physical properties of ferrites, Adv. Electron. El. M 6 (1954) 69
4. P.A., Miles, W.B., Westphal,and Von Hippel, A., Dielectric spectroscopy of ferromagnetic semiconductors, Rev. Mod. Phys. 29 (1957) 279
5. J.L., Snoek, Dispersion and absorption in magnetic ferrites at frequencies above one Mc/s, Physics.14 (1948) 207
6. S.M.Hoque M.A.Choudhury, and M.F.Islam, Characterization of Ni–Cu mixed spinel ferrite, J. Magn.Magn.Mater.251 (2002) 292
7. Liu,H.Zhu, Y.Yang,L., Bao, N., Ding, J., Chen, J., and K. Yu, Critical control of highly stable nonstoichiometric Mn–Zn ferrites with outstanding magnetic and electromagnetic performance for gigahertz high-frequency applications, ACS Appl. Mater. Interfaces.12(2020)16609
8. S. B.Narang, and Arora, A.: Broad-band microwave absorption and magnetic properties of M-type $Ba_{(1-2x)}La_xNa_xFe_{10}Co_{0.5}TiMn_{0.5}O_{19}$ hexagonal ferrite in 18.0–26.5 GHz frequency range, J. Magn.Magn.Mater.473 (2019) 272
9. Gubbala, S., Nathani, H., Koizol, K.and Misra, R.D.K., Magnetic properties of nanocrystalline Ni–Zn, Zn–Mn, and Ni–Mn ferrites synthesized by reverse micelle technique, Physica.B.348 (2004) 317
10. S.A., Saafan, T.M., Meaz, E.H., El-Ghazzawy, M.K., El Nimr, M.M., Ayad, and Bakr, M., AC and DC conductivity of NiZn ferrite nanoparticles in wet and dry conditions, J. Magn. Magn. Mater. 322 (2010) 2369
11. Singhal, S.and K. Chandra, Cation distribution and magnetic properties in chromium-substituted nickel ferrites prepared using aerosol route, J. Solid. State. Chem. 180 (2007) 296

12. Qiu, J., Wang, C.and Gu, M., Photocatalytic properties and optical absorption of zinc ferrite nanometer films, Mater. Sci. Eng. B 112 (2004) 1
13. Mathew, D.S., and Juang, R.S., An overview of the structure and magnetism of spinel ferrite nanoparticles and their synthesis in microemulsions, Chem.Eng.J.129(2007) 51
14. Patil, K.C., Hegde, M.S.,T.Rattan, and S.T.Aruna, Chemistry of nanocrystalline oxide materials, World Scientific(2008) London,UK
15. Chick, L.A., Pederson, L.R., Maupin, G.D., Bates, J.L., Thomas, L.E.and Exarhos, G.J., Glycine-nitrate combustion synthesis of oxide ceramic powders, Mater. Lett.10 (1990)6
16. S.Chikazumi, Physics of ferromagnetism, Oxford University Press(2009) New York,USA
17. S.M., Chavana, M.K., Babrekarc, S.S., Moreb,and Jadhavc, K.M., Structural and optical properties of nanocrystalline Ni–Zn ferrite thin films, J. Alloy.Compd 507 (2010) 21
18. P.A., Jadhav, R.S., Devan, Y.D.Kolekar,and Chougule, B.K., Structural, electrical and magnetic characterizations of Ni–Cu–Zn ferrite synthesized by citrate precursor method, J. Phys. Chem. Solids 70.(2009)396
19. G.F., Dionne, Molecular field coefficients of substituted yttrium iron garnets,J. Appl. Phys. 41 (1970) 4874
20. Dimri, M.C., Verma, A., Kashyap, S.C., Dube, D.C., Thakur, O.P., and Prakash, C., Structural, dielectric and magnetic properties of NiCuZn ferrite grown by citrate precursor method, Mater. Sci. Eng., B 133 (2006) 42
21. H.M.Zaki, Structure, analysis and some magnetic properties for low temperature fired Ni–Cu ferrite, Physica B. 407(2012) 2025
22. Upadhyay, C., Verma, H.C.and Anand, S., Cation distribution in nanosized Ni–Zn ferrites, J. Appl. Phys. 95 (2004) 5746
23. Yan, S., Yin, J.,and E.Zhou, Study on the synthesis of NiZnCu ferrite nanoparticles by PVA sol–gel method and their magnetic properties, J. Alloy.Compd.450 (2008)417
24. Tawfik, A.and Hemeda, O.M., Effect of vacancy jump rate on the permeability and dielectric properties of Ni0. 65Zn0. 35CuxFe2 – XO4, Mater. Lett.56 (2002) 665
25. T.Raghavender, A.,N.Biliskov, and Z.Skoko,XRD and IR analysis of nanocrystalline Ni–Zn ferrite synthesized by the sol–gel method, Mater. Lett.65(2011) 677
26. Singh, N., Agarwal, A., Sanghi, S., and Singh, P., Effect of magnesium substitution on dielectric and magnetic properties of Ni–Zn ferrite, Physica B. 406(2011) 687
27. Azadmanjiri, J., Salehani, H.K., Barati, M.R., Farzan, F., Preparation and electromagnetic properties of Ni1 – xCuxFe2O4 nanoparticle ferrites by sol–gel auto-combustion method, Mater. Lett. 61 (2007) 84
28. R.B., Kale, C.D., Lokhande, Influence of air annealing on the structural, optical and electrical properties of chemically deposited CdSe nano-crystallites, Appl. Surf. Sci. 223 (2004) 343

Tables

Table.1.XRD pattern data of samples.

sample	Θ(°)	crystallite size(A°)	lattice strain	lattice constant(A°)	crystalline percentage	wavenumber of tetrahedral sites (cm^{-1})
Ni.7 Cu.3 Fe2 O4	41.67	393	0.248	8.352	831	560
Ni.5 Cu.5 Fe2 O4	41.60	475	0.239	8.353	79	558
Ni.3 Cu.7 Fe2 O4	41.61	449	0.253	8.385	77	548

Table.2. Magnetic data of samples.

sample	H_c(Oe)	M_r(emu/g)	M_s(emu/g)
Ni.7 Cu.3 Fe2 O4	70.26	9.48	48.51
Ni.5 Cu.5 Fe2 O4	65.76	9.65	47.98
Ni.3 Cu.7 Fe2 O4	45.32	7.55	55.30

Figures

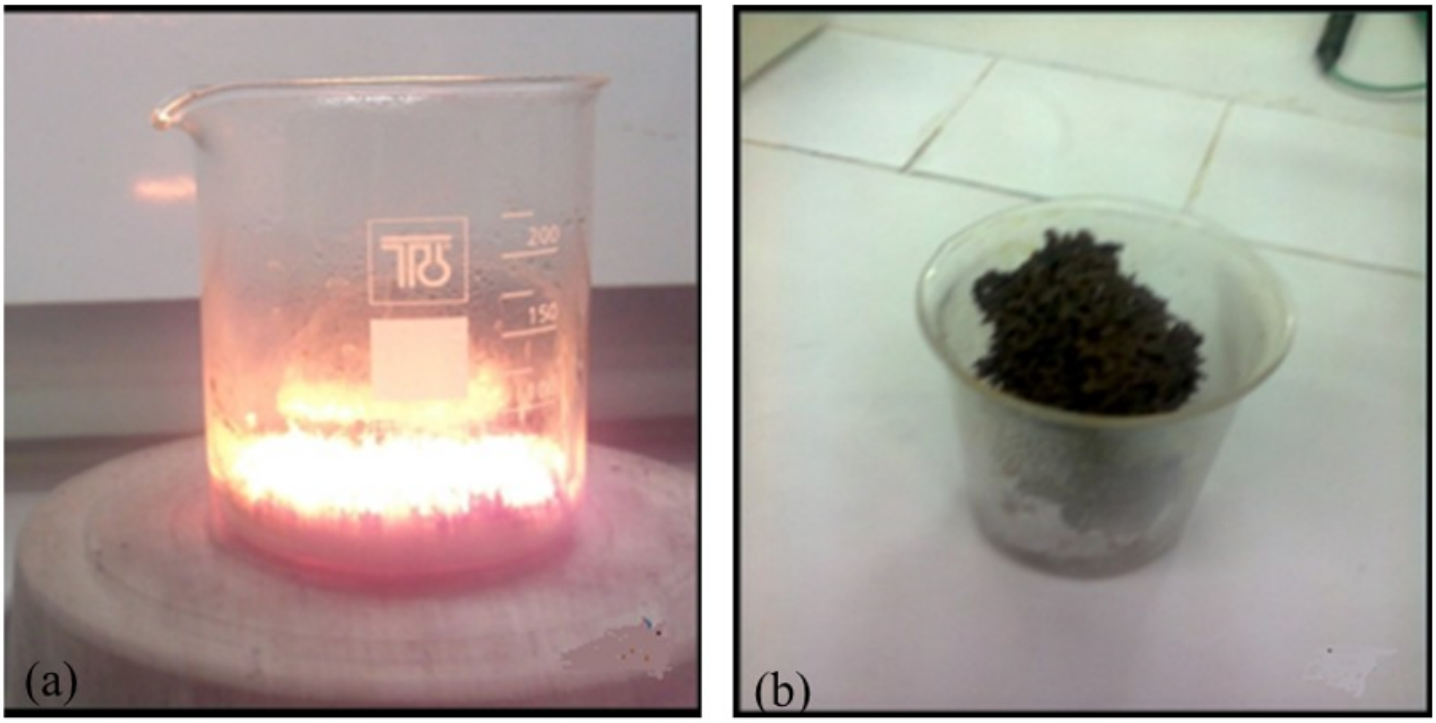

Figure 1

(a) an image of combustion, (b) fabricated ferrite in our work.

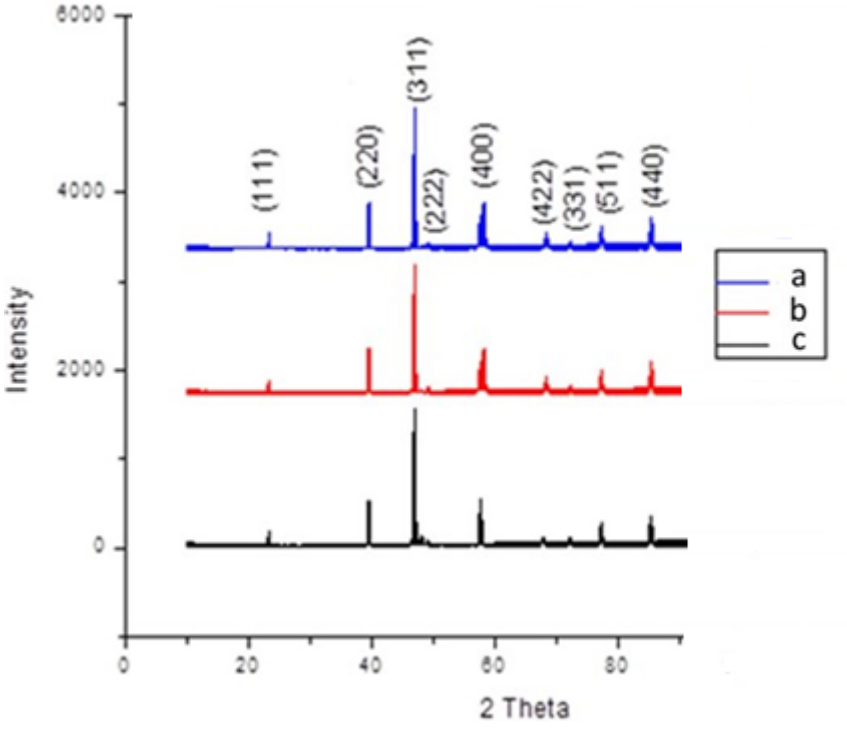

Figure 2

XRD patterns of ferrite nanoparticles (a) Ni.7Cu.3 Fe2O4, (b) Ni.5Cu.5 Fe2O4, (c) Ni.3Cu.7 Fe2O4.

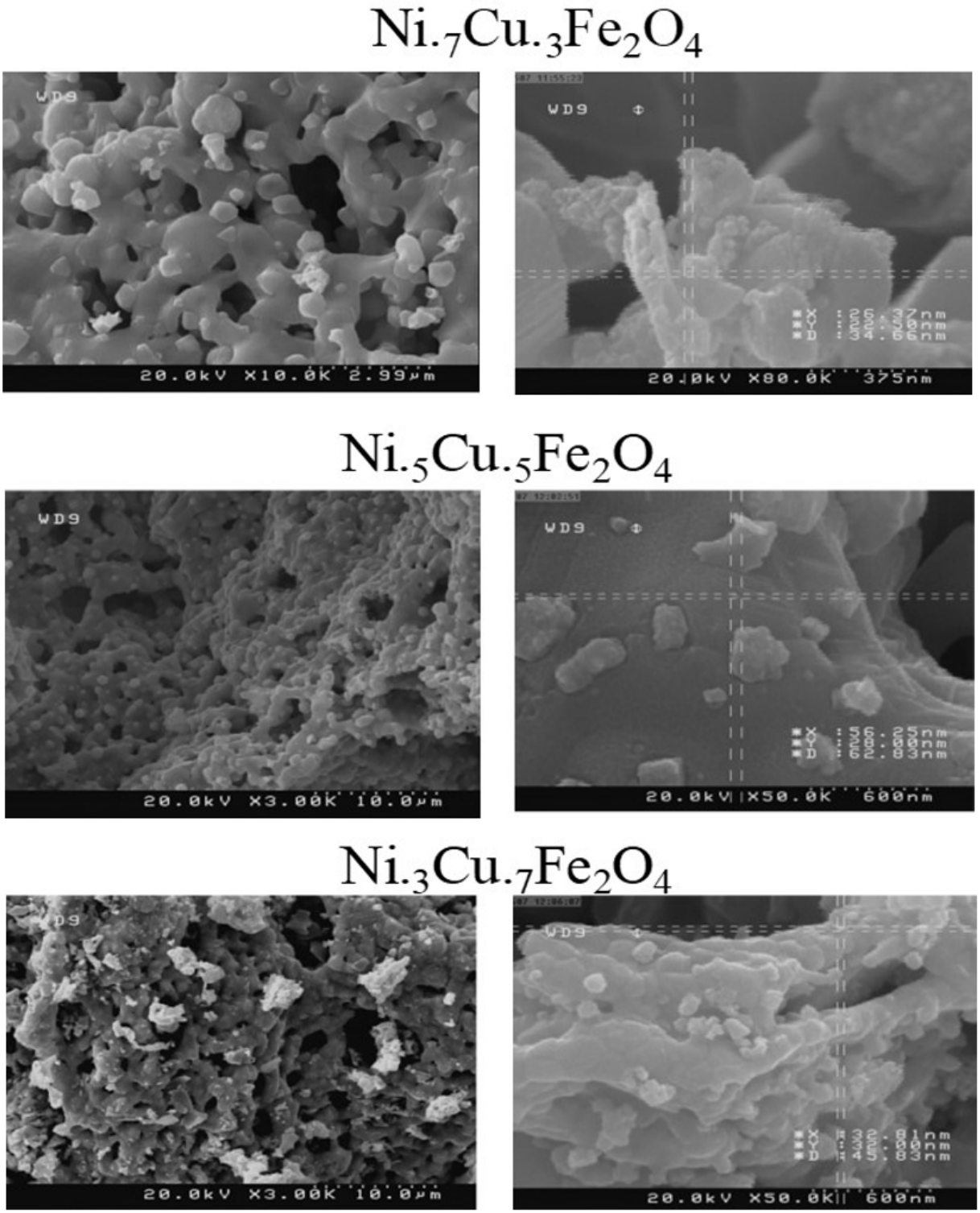

Figure 3

FESEM electron micrographs of surface Nickel-Copper ferrite with three percent by weight.

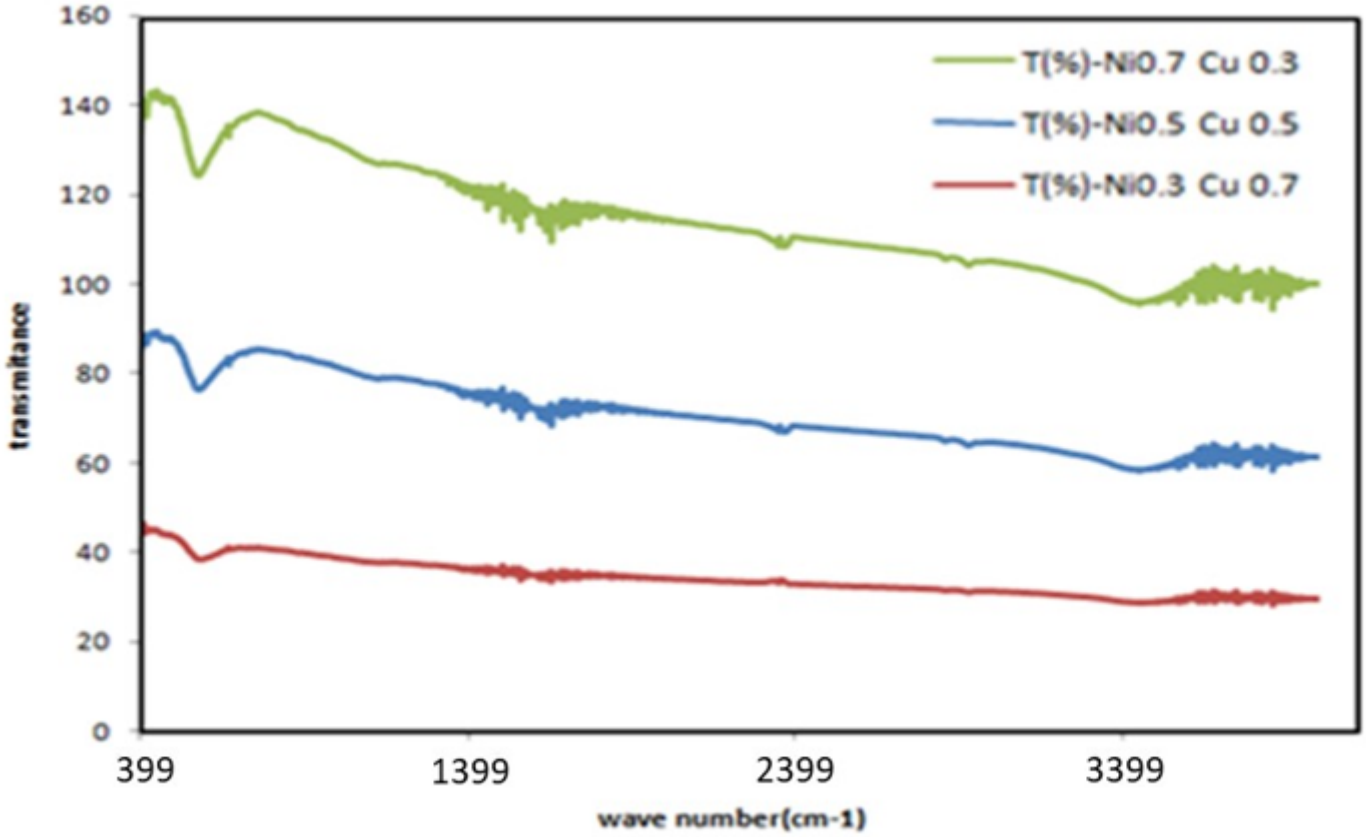

Figure 4

FTIR transmission spectra of Nickel-Copper ferrite with different weight percentages.

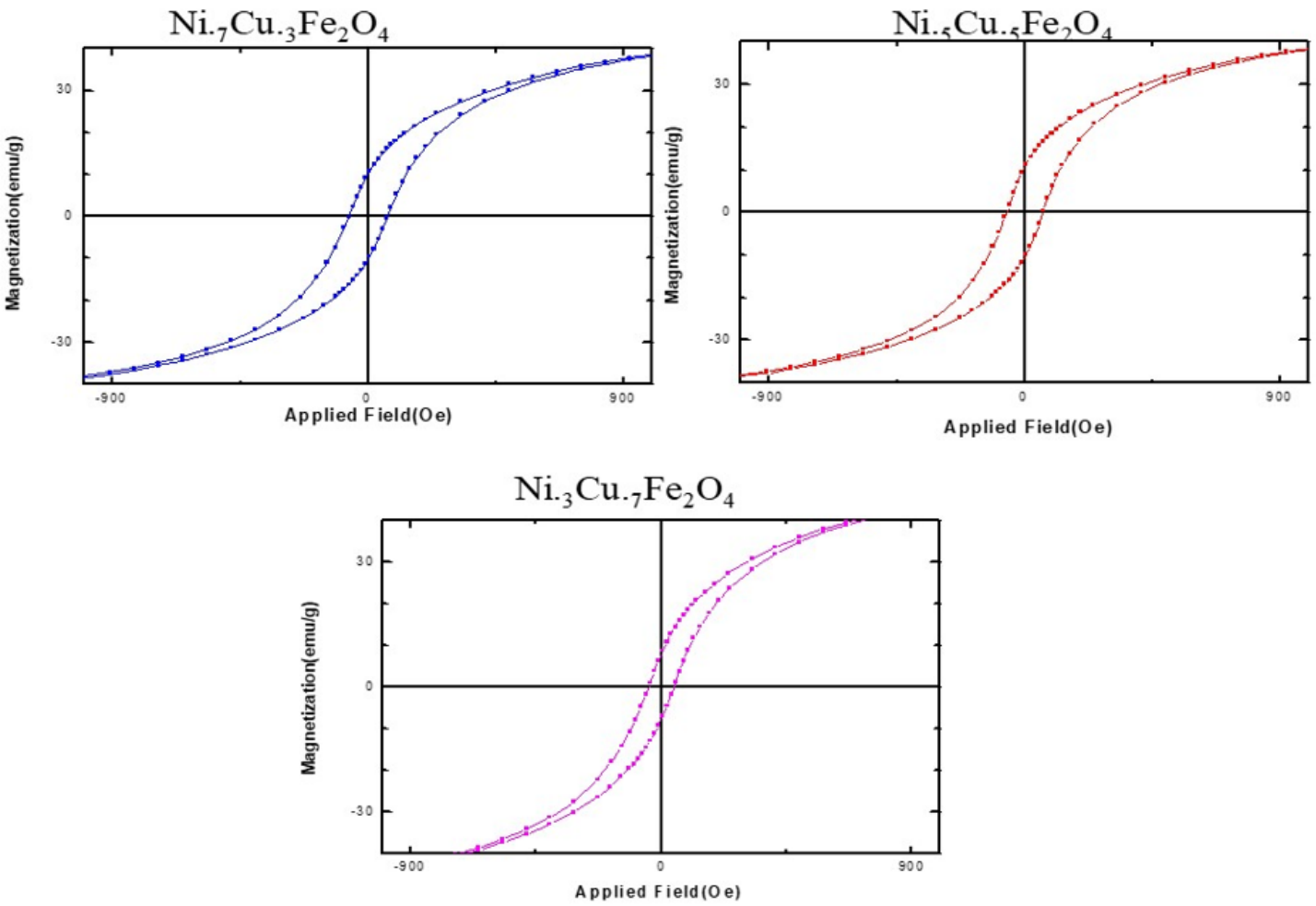

Figure 5

The hysteresis loop of Nickel-Copper ferrite with different weight percentages.

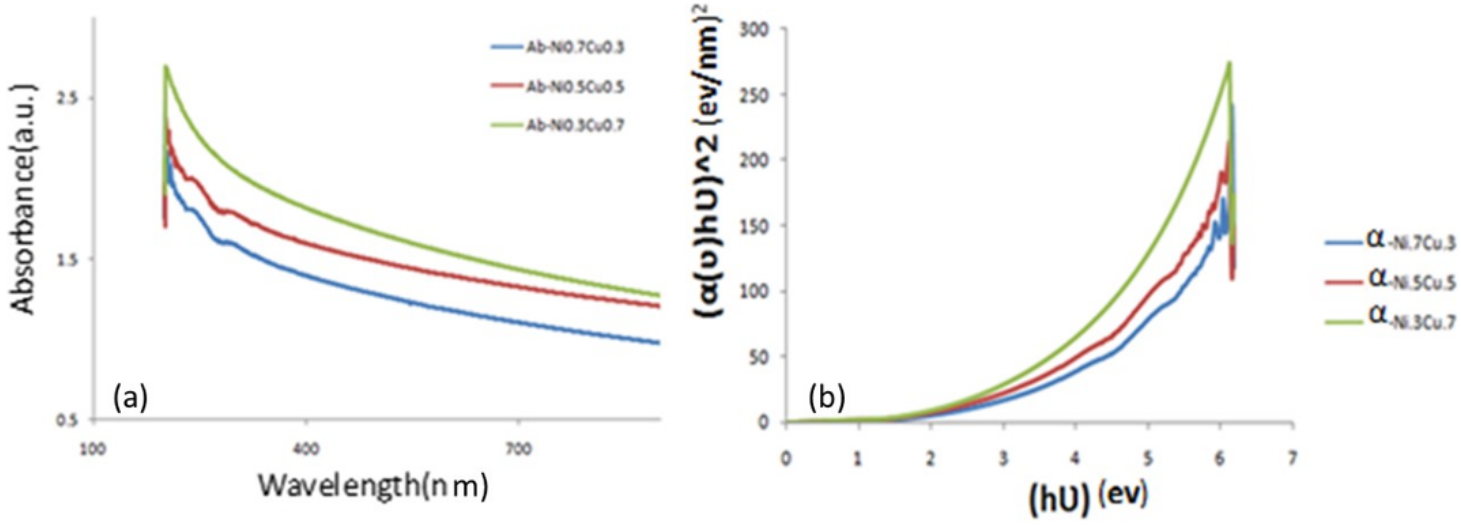

Figure 6

(a) Optical absorbance UV of samples, (b) absorbance coefficient of samples.